Static contact angle in lattice Boltzmann models of immiscible fluids

M. Latva-Kokko and Daniel H. Rothman
Department of Earth Atmospheric and Planetary Sciences, Massachusetts Institute of Technology, 77 Massachusetts Avenue, Cambridge, Massachusetts 02139-4307, USA
(Received 27 April 2005; published 3 October 2005)

We study numerically the capillary rise between two horizontal plates and in a rectangular tube, using a lattice Boltzmann (LB) method. We derive an equation for the static fluid-solid contact angle as a function of the wetting tendency of the walls and test its validity. We show that the generalized Laplace law with two independent radii of curvature is followed in capillary rise in rectangular tubes. Our method removes the history dependence of the fluid-solid contact angle that had been present in earlier LB schemes.

DOI: 10.1103/PhysRevE.72.046701 PACS number(s): 47.11.+j, 47.55.Kf, 68.08.Bc, 47.60.+i

I. INTRODUCTION

Wetting and capillary phenomena are abundant in nature and technological applications. Flow of oil and water through subsurface reservoirs and the rise of nutrient-rich fluids in the stem of a plant are two examples of systems where capillary forces strongly influence the flow. These capillary forces are determined by wetting of the solid phase by the two fluid phases involved. The wetting ability is controlled by the pairwise interfacial energies of the two fluids and the solid, and it can be characterized by a contact angle. The contact angle θ is the angle formed by the intersection of the interfaces bounding the three phases.

In experimental fluid mechanics the determination of the static contact angle requires very clean conditions [1,2]. In many practical situations one finds that the three phase contact line is pinned and immobile not only for a single θ but whenever θ lies in an interval

$$\theta_r < \theta < \theta_a. \tag{1}$$

The angle θ_r is called the receding contact angle and the angle θ_a is called the advancing contact angle [1]. It is mentioned in Ref. [1] that $\theta_a - \theta_r$ may be as large as 10° or more for surfaces that have not been specially prepared. Fermigier and Jenffer [3] report a much larger 30°–60° contact angle hysteresis in the case of glycerine-silicon oil systems. Also Stokes *et al.* [4] report a 20° contact angle hysteresis in the case of a glycerol-methanol mixture. It is unclear what causes this contact angle hysteresis. It seems that the effect is much more pronounced in the case of a liquid-liquid interface than in a liquid-gas interface. There have been many proposed explanations for the contact angle hysteresis, but it is generally believed that properties of the surface cause this effect. Properties such as surface roughness, chemical contaminations or inhomogeneties, and solutes have been shown to have an effect on the static contact angle.

Two-phase fluid flow in confined geometries is strongly influenced by capillary effects (see e.g., Refs. [5–11]). The change in the aperture of the flow channel leads to change in the curvature of the fluid-fluid interface. This in turn leads to change in the capillary pressure over the interface as predicted by the Laplace law,

$$\Delta P = \sigma \cos\theta \left(\frac{1}{r_1} + \frac{1}{r_2} \right). \tag{2}$$

Here ΔP gives the pressure drop across the interface, σ is the surface tension, and r_1 and r_2 are the principle radii of curvature of the interface.

We seek to understand the dynamics of a moving interface in confined geometries. Specifically, we study the manifestation of this problem in lattice Boltzmann (LB) methods of immiscible fluids. Our first goal is to understand what sets the shape of the LB fluid-fluid interfaces in static or quasistatic situations. We show how an equation for the contact angle in the case of partial wetting can be derived from first principles. The surface curvature is measured in the case of rectangular tubes and we find the mean curvature to be constant also in the case of two independent finite radii of curvature. We also show that the LB method [12] follows the generalized form of Laplace law given by Eq. (2). In a previous paper we reported an effect called lattice pinning for the lattice Boltzmann color-gradient method [12]. This effect leads to contact angle hysteresis as we shall demonstrate in this paper. We report a 19° contact angle hysteresis and show that an improved method [12] has no contact angle hysteresis.

This paper is organized as follows. In Sec. II the LB method is introduced with a brief review of a modified method that removes lattice pinning. In Sec. III we present a first-principles derivation of the contact angle in LB models. In Sec. IV we study the capillary rise in a two-dimensional capillary tube and show how the contact angle depends on the history of the system if the problem of lattice pinning is not removed. In Sec. V we use the improved method for the capillary rise in rectangular capillary tubes and show that our method provides the right contact angles on the walls and that the Laplace law is followed across interfaces that have two independent finite radii of curvature. Section VI contains the concluding remarks.

II. METHOD

The fundamental idea of the LB method is to construct simplified kinetic models that incorporate the essential physics of microscopic or mesoscopic processes. Macroscopic or

hydrodynamic behavior naturally emerges as a result of these kinetics. The LB method [13–16] is constructed on a regular lattice. At each lattice point the populations $N_i^\sigma(\mathbf{x},t)$ are known. The subscript i denotes the lattice direction $\mathbf{c}_i$ connecting two neighboring lattice sites, the superscript σ denotes the particle type (red or blue), $\mathbf{x}$ is the position in the lattice, and t is the simulation time step. These give the density, the velocity, and the pressure and/or stress of the fluid at a given point.

We use the standard Bhatnagar-Gross-Krook (BGK)-collision scheme with a single relaxation time. Each simulation time step consists of the following steps:

(1) Propagation. Particle populations hop to neighboring sites, $N_i^\sigma(\mathbf{x}+\mathbf{c}_i,t)=N_i^{\sigma\prime}(\mathbf{x},t-1)$.

(2) Calculation of pseudoequilibrium populations $N_i^{(\mathrm{eq})}$,

$$N_i^{(\mathrm{eq})}(\rho,\mathbf{u}) = \rho\left[\tfrac{1}{36} + \tfrac{1}{12}\mathbf{c}_i\cdot\mathbf{u} + \tfrac{1}{8}\mathbf{c}_i\mathbf{c}_i{:}\mathbf{u}\mathbf{u} - \tfrac{1}{24}\mathbf{u}\cdot\mathbf{u}\right], \quad (3)$$

$$N_0^{(\mathrm{eq})}(\rho,\mathbf{u}) = \rho\left[\tfrac{1}{3} - \tfrac{1}{2}\mathbf{u}\cdot\mathbf{u}\right], \quad (4)$$

$\rho=\Sigma_{i,\sigma}N_i^\sigma$ is the number of particles and $\mathbf{u}$ is the fluid velocity. The pseudoequilibrium populations are chosen in such a way that in the long-wavelength limit the Navier-Stokes equations with an ideal gas equation of state are obtained [16].

(3) Collision. The populations $N_i=N_i^{\mathrm{red}}+N_i^{\mathrm{blue}}$ relax towards the pseudoequilibrium distributions,

$$N_i'(\mathbf{x},t) = (1+\lambda)N_i(\mathbf{x},t) - \lambda N_i^{(\mathrm{eq})}(\mathbf{x},t). \quad (5)$$

Here λ is a relaxation parameter which acts as an inverse relaxation time. It also sets the value of kinematic viscosity, i.e., $\nu=-\frac{1}{3}\left[(1/\lambda)-\frac{1}{2}\right]$ [16]. These collision and relaxation rules lead to the following macroscopic mass and momentum equations [16]

$$\partial_t\rho + \boldsymbol{\nabla}\cdot\mathbf{v} = 0, \quad (6)$$

$$\partial_t\mathbf{v} + \mathbf{v}\cdot\boldsymbol{\nabla}\mathbf{v} = -\boldsymbol{\nabla}p + \nu\nabla^2\mathbf{v}, \quad (7)$$

where $\rho=\Sigma_{i,\sigma}N_i^\sigma$, $p=\frac{1}{3}\rho$, and $\mathbf{v}=\rho\mathbf{u}$.

(4) External forces. Addition of, e.g., gravity or a pressure gradient.

(5) Surface tension. Interfacial dynamics are incorporated by a modification [12,17] of the color-gradient based method of Gunstensen *et al.* [18]. First surface tension is introduced by changing the distributions

$$N_i''(\mathbf{x},t) = N_i'(\mathbf{x},t) + A|\mathbf{f}(\mathbf{x},t)|\left(\frac{(\mathbf{c}_i\cdot\mathbf{f})^2}{\mathbf{f}\cdot\mathbf{f}} - \frac{1}{2}\right), \quad (8)$$

where A is the parameter that sets the magnitude of the surface tension [16,18] and the color-gradient is defined as

$$\mathbf{f}(\mathbf{x},t) = \sum_i \mathbf{c}_i \sum_j \left[N_j^{\mathrm{red}}(\mathbf{x}+\mathbf{c}_i,t) - N_j^{\mathrm{blue}}(\mathbf{x}+\mathbf{c}_i,t)\right]. \quad (9)$$

Then color is redistributed according to [12]

$$N_i^{\mathrm{red}\prime} = \frac{N^{\mathrm{red}}}{\rho}N_i'' + \beta\frac{N^{\mathrm{red}}N^{\mathrm{blue}}}{\rho^2}N_i^{(\mathrm{eq})}(\rho,0)\cos\varphi, \quad (10)$$

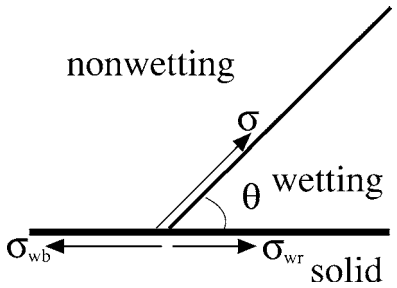

FIG. 1. Force balance at the three-component contact line.

$$N_i^{\mathrm{blue}\prime} = \frac{N_i^{\mathrm{blue}}}{\rho}N_i'' - \beta\frac{N^{\mathrm{red}}N^{\mathrm{blue}}}{\rho^2}N_i^{(\mathrm{eq})}(\rho,0)\cos\varphi. \quad (11)$$

Here $N^{\mathrm{red}}=\Sigma_i N_i^{\mathrm{red}}$ and $N^{\mathrm{blue}}=\Sigma_i N_i^{\mathrm{blue}}$ are the total numbers of red and blue particles at a given site and $N_i^{(\mathrm{eq})}(\rho,0)$ is the zero-velocity equilibrium distribution, β is a parameter giving the tendency of the two fluids to separate, and φ is the angle between the color gradient $\mathbf{f}$ and the direction $\mathbf{c}_i$.

We use a simple bounce-back rule [16,19] on the walls. This rule leads to a no-slip boundary condition approximately halfway between the wall node and the nearest fluid node [16,19]. The wetting tendency of the walls is controlled by a single parameter $p_{\mathrm{red}}\geqslant 0$ that measures the fraction of red color on the solid nodes compared to the density of the surrounding fluid phase. Combined with Eqs. (8) and (9) this will give rise to a color gradient, and hence surface tension at the walls. When the simulation is initialized we place red color on the walls for the purpose of calculating the color gradient. The amount of red color on the walls is

$$N_{\mathrm{redwall}} = \rho p_{\mathrm{red}}, \quad (12)$$

where ρ is the density of the fluid phase. The red fluid is the wetting fluid and we have complete wetting for $p_{\mathrm{red}}\geqslant 1.0$, partial wetting for $0<p_{\mathrm{red}}<1$, and neutral wetting for $p_{\mathrm{red}}=0$.

III. DERIVATION OF THE CONTACT ANGLE

Theoretical estimates of the contact angle in LB color-gradient methods can be found by a simple force balance or by a detailed derivation starting from the dynamics of the model. To our knowledge these calculations have not been previously presented. We present both derivations here.

A. Force balance

The force balance at the three-phase contact line states,

$$F\cos\theta + F_{wr} = F_{wb}. \quad (13)$$

Here F is the force imposed by the fluid-fluid surface tension, θ is the contact angle, F_{wr} is the force imposed by the wall-red fluid (wetting fluid) surface tension and F_{wb} is the force imposed by the wall-blue fluid (nonwetting fluid) surface tension. This is shown schematically in Fig. 1. First, note that each of these forces is proportional to the associated surface tension with the same proportionality factor. Second,

note that the surface tension is proportional to the amount by which the distributions are perturbed in the recoloring step. This is given by Eq. (8) and is proportional to the color gradient. In fact as we will see in the case of the detailed derivation the total magnitude of the surface tension is proportional to the sum of the magnitudes of the color gradient in a line perpendicular to the interface. In the case of sharp interfaces this can be evaluated at the interface. For the red fluid–blue fluid interface it is given by Eq. (9) as $|\mathbf{f}|=N^{\mathrm{red}}+N^{\mathrm{blue}}=\rho+\rho=2\rho$, where ρ is the density of both the red and the blue fluid. For the red fluid and/or wall interface it is $|\mathbf{f}|_{wr}=|N^{\mathrm{red}}-N_{\mathrm{redwall}}|=\rho(1-p_{\mathrm{red}})$, and for the blue fluid and/or wall interface it is $|\mathbf{f}|_{wb}=N^{\mathrm{blue}}+N_{\mathrm{redwall}}=\rho(1+p_{\mathrm{red}})$. If these are combined with Eq. (13) we obtain

$$2\rho\cos\theta+\rho(1-p_{\mathrm{red}})=\rho(1+p_{\mathrm{red}}), \tag{14}$$

i.e.,

$$\cos\theta=p_{\mathrm{red}}. \tag{15}$$

Since the fluids are identical in all other respects than their interaction with the wall, making one fluid wetting automatically makes the other one nonwetting. Also, since the color-gradient in Eq. (9) only depends on the difference $N^{\mathrm{red}}-N^{\mathrm{blue}}$, coloring the walls negative red has the same effect as coloring them blue. Hence Eq. (15) works for all $-1\leqslant p_{\mathrm{red}}\leqslant 1$.

B. Microdynamical basis

We now provide a derivation based on the lattice dynamics [12,16,18,20]. We begin with the mechanical definition of surface tension [21]

$$\sigma=\int_{-\infty}^{\infty}(P_N-P_T)dz, \tag{16}$$

where P_N and P_T are normal and tangential components of the pressure tensor. These are given by [16,22]

$$P_N=\sum_{i=1}^{18}N_i c_{iN}c_{iN}, \tag{17}$$

$$P_T=\sum_{i=1}^{18}N_i c_{iT}c_{iT}, \tag{18}$$

where c_{iN} and c_{iT} are components of the lattice directions $\mathbf{c_i}$ normal and tangential to the interface. The surface tension is given by [12,16,18,20]

$$\sigma=-\frac{8A}{\lambda}\sum_{\mathbf{x}}|\mathbf{f}|. \tag{19}$$

Here the sum $\Sigma_{\mathbf{x}}$ runs across the interface on a line perpendicular to it.

What then is $\Sigma_{\mathbf{x}}|\mathbf{f}|$? Without loss of generality one may consider an interface oriented in the x,y plane. Consider a sharp interface for which all sites above some z are totally blue and all sites below are totally red. Now we can calculate $\Sigma_{\mathbf{x}}|\mathbf{f}|$. Only the two sites on the interface contribute to the sum. For the bottom site the color gradient is pointing down and its magnitude is

$$4\times\rho+2\times\rho+4\times\rho+2\times\rho=12\rho \tag{20}$$

(the diagonal directions pointing down, the $-z$ direction, the diagonal directions pointing up, the z direction). The same is true for the top site, which makes

$$\sum_{\mathbf{x}}|\mathbf{f}|=24\rho. \tag{21}$$

This value of surface tension is also true for any interface of any width that starts from $N^{\mathrm{red}}=\rho$ and $N^{\mathrm{blue}}=0$ and ends at $N^{\mathrm{red}}=0$ and $N^{\mathrm{blue}}=\rho$, and has a constant direction of the color gradient. The reason for this is that the sum of gradients such as $\Sigma_{\mathbf{x}}|\mathbf{f}|$ depends only on the amount of red and blue particles at the ends of the summation, whereas all the intermediate steps cancel out. This is demonstrated by an alternative derivation for the surface tension given in Ref. [16]. Substituting Eq. (21) to Eq. (19) we obtain [16,18,20]

$$\sigma=-192A\rho/\lambda. \tag{22}$$

We next do the same calculation for the wall. Consider a sharp interface. In the case of red fluid and/or wall we get

$$|\mathbf{f}|=4\rho+2\rho-4p_{\mathrm{red}}\rho-2p_{\mathrm{red}}\rho=6(1-p_{\mathrm{red}})\rho \tag{23}$$

for the fluid site immediately below the wall. Because of the bounce back rule these distributions are exactly mirrored by the wall sites giving

$$\sum_{\mathbf{x}}|\mathbf{f}|=12(1-p_{\mathrm{red}})\rho. \tag{24}$$

In the case of blue fluid and/or wall we get

$$|\mathbf{f}|=4\rho+2\rho+4p_{\mathrm{red}}\rho+2p_{\mathrm{red}}\rho=6(1+p_{\mathrm{red}})\rho \tag{25}$$

for the fluid site immediately below the wall and by reflection

$$\sum_{\mathbf{x}}|\mathbf{f}|=12(1+p_{\mathrm{red}})\rho. \tag{26}$$

Combining this with Eq. (13) we find

$$24\rho\cos\theta-12(1-p_{\mathrm{red}})\rho=12(1+p_{\mathrm{red}})\rho, \tag{27}$$

i.e.,

$$\cos\theta=p_{\mathrm{red}}. \tag{28}$$

If the fluid-fluid interface is not sharp the results in (24) and (28) are not accurate. Instead, because the bounce-back rule mirrors the distributions at the fluid sites right next to the walls, the fluid and/or wall surface tension depends on the amount of blue and red fluid at these sites. Since these depend (because of lattice pinning [12]) on how the lattice is initialized this can create static contact angle hysteresis. This could in principle be removed by changing the wall distributions, but unfortunately then we could no longer be certain of the no-slip boundary condition. This incompatibility of the no-slip boundary condition with the fluid and/or wall surface tension [23] and finite interfacial width can therefore lead to contact angle hysteresis in LB color gradient methods.

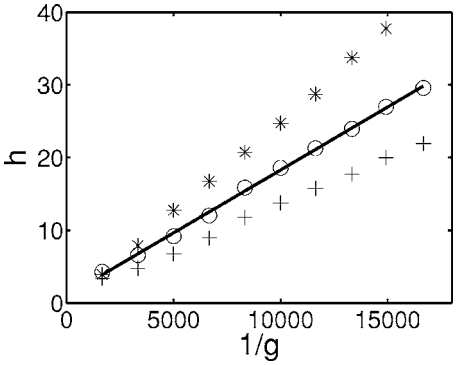

FIG. 2. Capillary rise heights. The circles denote the capillary rise height for both drainage and imbibition in the case where we use the improved color gradient method [12]. In this case the data matches the prediction of (29) with a contact angle 60°. The asterisk denotes the equilibrium height in the case of drainage, where we used the color gradient method of Gunstensen *et al.* [18]. These would fit Eq. (29) with a contact angle of 49°. The plus signs denote equilibrium height in the case of imbibition, again using Gunstensen's method [18]. These would fit with a contact angle of 68°.

IV. MEASURING THE CONTACT ANGLE

In this section we study the capillary rise in a simple two-dimensional situation of a straight tube. One of the fluids (red) is wetting and fills the bottom part of the tube. We apply a constant body force $(-mg\hat{\mathbf{z}})$ to that fluid and no body force to the other (blue) fluid, and measure the equilibrium surface height as a function of g and the width of the tube.

Since the wetting fluid is subject to a gravity-type body force the hydrostatic pressure drop $\Delta p_{\text{hydro}}=\rho g h$ must be equal to the capillary pressure drop accross the interface $\Delta p_{\text{cap}}=2\sigma\cos\theta/x$, where x is the width of the tube and σ is the surface tension. These combine to give the equilibrium height h [24], where

$$h=\frac{2\sigma\cos\theta}{\rho x g}. \tag{29}$$

In Fig. 2 we plot the capillary rise heights for different body forces, i.e., changing g. We use g ranging from 6.0×10^{-5} to 6.0×10^{-4}, relaxation parameter $\lambda=-1.0$, density $\rho=10.0$, $p_{\text{red}}=0.5$, $A=1.0\times10^{-4}$ giving surface tension $\sigma=0.192$, and width $x=10$. Equation (28) gives the theoretical value of the contact angle as $\theta=\cos^{-1}(p_{\text{red}})=60°$. We call the invasion of the wetting fluid to a capillary filled with a nonwetting imbibition and the invasion of the nonwetting fluid to a capillary filled with wetting fluid drainage. The contact angle above which imbibition is possible is called the advancing contact angle θ_a and the contact angle below which drainage is possible is called the receding contact angle θ_r. The equilibrium height of the interface is the same for both drainage and imbibition when the improved color gradient method [12] was used. This implies that $\theta_a=\theta_r$ for the improved color gradient method and there is no contact angle hysteresis. This height as a function of $1/g$ is plotted as circles. The straight line gives the theoretical prediction with $\theta=60°$. Similar accord with theory also occurs with wetting tendencies p_{red} ranging from 0.1 to 1.0.

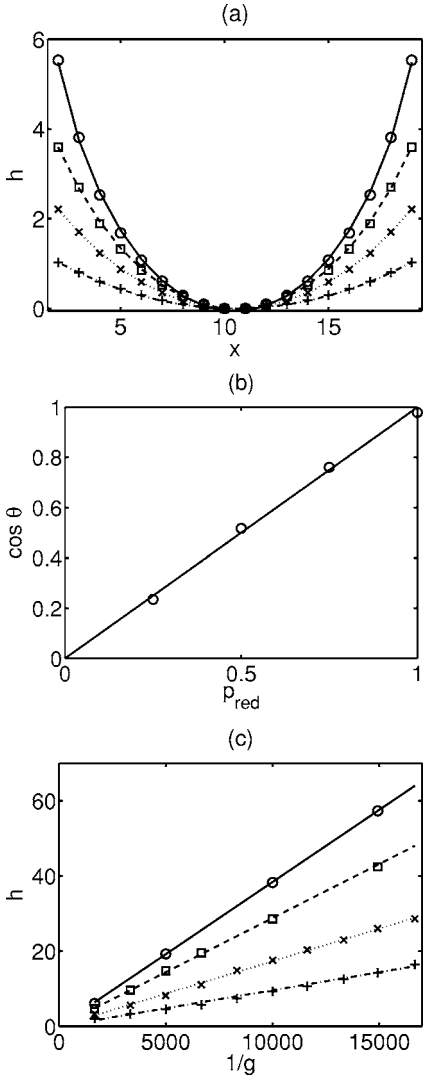

FIG. 3. Evaluation of static contact angle. In (a) we show the fluid-fluid interface for $p_{\text{red}}=0.25$, 0.5, 0.75, and 1.0. The curves shown are circular fits. In (b) we show the contact angles given by these fits (○) as a function of wetting tendency p_{red}. For comparison the prediction given by Eq. (28) is shown by the straight line. In (c) we confirm these results by measuring the capillary rise height and comparing them to the predictions (straight lines) given by Eq. (29). For (a) and (c) plus signs and dashed-dotted line denote $p_{\text{red}}=0.25$; crosses and dotted line denote $p_{\text{red}}=0.5$; squares and dashed line denote $p_{\text{red}}=0.75$; and circles and solid line denote $p_{\text{red}}=1.0$.

In Fig. 3 we further demonstrate the validity of Eq. (28). We measure the static contact angle as a function of wetting tendency p_{red} by fitting a circle to the fluid-fluid interface. The radius of this circle is directly related to the contact angle [16,24], so that

$$R=\frac{x}{2\cos\theta}, \tag{30}$$

where R is the radius. These fits are shown in Fig. 3(a) for four different wetting tendencies $p_{\text{red}}=0.25$, 0.5, 0.75, and 1.0. In Fig. 3(b) we compare the measured static contact angles to the prediction given by (28). Figure 3(c) shows the

height of the capillary rise as predicted by Eq. (29) for these wetting tendencies.

The good fits in Figs. 2 and 3 between theory and simulations is a consequence of the improved recoloring algorithm introduced in Ref. [12]. Had those improvements not been made we would have lattice-pinning induced contact angle hysteresis. In the case of imbibition the contact angle on the walls is as high as $\theta_a=68°$. In the case of drainage the contact angle is $\theta_r=49°$. In fact one can have any static contact angle between 49° and 68° depending on the initial conditions. In experimental situations (see, e.g., Refs. [1,2]) the receding and advancing contact lines do not have the same contact angle. In some situations it may be beneficial to use a model that has appreciable contact angle hysteresis. In those situations the recoloring scheme suggested by Gunstensen [18] may be more useful than the improved recoloring scheme.

V. RECTANGULAR CAPILLARY TUBES

We now test the applicability of our method for fluid flow simulations in complex geometries. In order to do this we check that the pressure drop over the interface matches the prediction of the Laplace law. In the case of the spherical bubble the well known and widely tested [16] relation between the pressure drop and the radius of curvature is $\Delta p = p_{\text{inside}} - p_{\text{outside}} = 2\sigma/r$, where r is the radius of the bubble. We first applied this bubble test to our method and found excellent agreement.

In general, however, the Laplace law depends on two radii of curvature, r_1 and r_2, such that

$$\Delta p_{\text{interface}} = \sigma(1/r_1 + 1/r_2). \tag{31}$$

Below we verify this general relation when the surface has two finite independent radii of curvature. To do this we used rectangular capillary tubes.

The exact solution of the interface shape in a rectangular tube is far from a trivial problem [25–28]. Nevertheless it provides an excellent test case for two independent finite radii of curvature. There are different methods of testing whether the pressure drop over the interface is accurate. The easiest is a simple force balance equation,

$$\Delta p x y = (2x + 2y)\sigma \cos\theta, \tag{32}$$

where x is the size of the rectangular capillary tube in the x direction, y is the size of the rectangular capillary tube in the y direction, and

$$\Delta p = 2\sigma \cos\theta \left(\frac{x+y}{xy}\right). \tag{33}$$

Note however that this equation only gives the sum of the two radii of curvature.

In the case of a rectangular capillary tube we first checked the validity of the force balance equation. Figure 4 shows these results. The solid lines are the estimated heights given by Eqs. (32) and (33) with a static contact angle $\theta=60°$. As one can see the assumption of a static contact angle does not change and the use of the equilibrium pressure difference

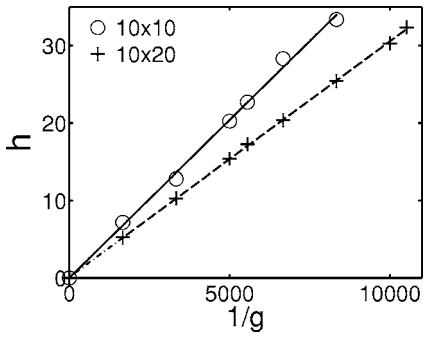

FIG. 4. Capillary rise heights for rectangular tubes. The circles denote the measured rise heights for 10×10 rectangular tube. The solid line is an estimate for the rise height given by Eqs. (32) and (33) when $x=10$, $y=10$, $\theta=60°$, and $\sigma=0.192$. The plus signs denote the measured rise heights for a 10×20 rectangular tube and the dashed line is the corresponding theoretical prediction for the case when $x=10$, $y=20$, $\theta=60°$, and $\sigma=0.192$.

given by Eq. (32) holds well. Because the position of the interface is difficult to measure close to the walls, this estimate contains a significant amount of uncertainty. Moreover the contact line on the walls is not rectangular.

We next show how the main radii of the curvature, r_1 and r_2, can be calculated from the surface data. In the case of a rectangular tube the center point of the tube is where the measurement of the two radii of curvature is the easiest. The surface normal at that point is directed in the same direction as the tube, and the two main axes are given by the short and the long direction. We fit two circular curves in these directions to find the radii of curvature. The results here are shown for a tube with a cross section of 10×20 lattice sites in Figs. 5 and 6. The radius of curvature is directly related to the contact angle [16,24], so that

$$r_i = \frac{w_i}{2\cos\theta}, \tag{34}$$

where $w_1=x=10.0$ and $w_2=y=20.0$. The best fit to the data gives $r_1=x/(2\cos\theta)=9.231$ and $r_2=y/(2\cos\theta)=18.68$. These would imply a contact angle given by $\cos\theta=0.487$ or $\cos\theta=0.508$. This is consistent with the value one gets from the force balance equation.

It is evident that the surface exhibits the right curvatures in given directions and that the pressure drop over the interface matches the Laplace law value. We therefore conclude that the method can be used to simulate imbibition and drainage in complex geometries, and that the mean curvature at any given point of the interface will give the interfacial pressure drop, and hence the interface dynamics.

We also find that if the numerical noise on the interface is smoothed out by either fitting an ellipsoidal surface or by calculating local averages one finds that the mean curvature on the interface stays constant. Since the mean curvature gives the pressure drop across the interface we also conclude that the pressure drop is constant. This corresponds with mechanical equilibrium. Thus the Laplace law is followed, in the case of two independent finite radii of curvature, and for

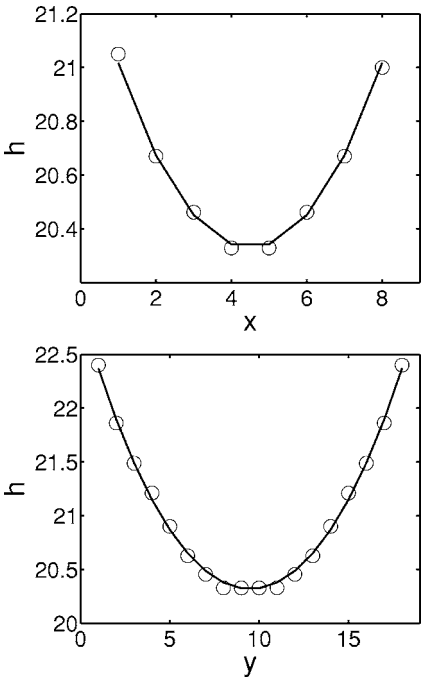

FIG. 5. Fits to the central part of the two fluid interface. On the top is the short side and on the bottom is the long side. The cross-sectional size of the tube is 10×20 lattice sites.

static interfaces the interfacial mean curvature remains constant.

VI. CONCLUSIONS

We have derived an estimate of the contact angle as a function of the wetting tendency of the walls when using color-gradient based LB models. We show that when using the improved method [12] this estimate gives the appropriate static contact angle for both imbibition and drainage. We have applied the method to the case of rectangular capillary tubes and showed that the contact angle remains constant and that the Laplace law is followed when the interface has two independent nonzero radii of curvature.

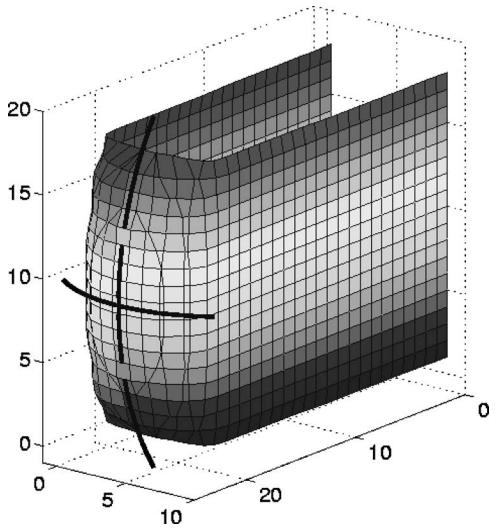

FIG. 6. The fits of Fig. 4 shown on the interface.

This work is a necessary precursor to understanding dynamical aspects of interface motion. Further work will consist of finding how contact angles vary as a function of the interfacial velocity and how the transition from quasistatic to dynamic flow takes place in capillaries with changing apertures.

ACKNOWLEDGEMENT

This work was supported by the Office of Science (BER), U.S. Department of Energy, Grant No. DE-FG07-02ER63490.

[1] P. G. de Gennes, Rev. Mod. Phys. **57**, 827 (1985).
[2] E. Schäffer and P. Z. Wong, Phys. Rev. E **61**, 5257 (2000).
[3] M. Fermigier and P. Jenffer, J. Colloid Interface Sci. **146**, 226 (1991).
[4] J. P. Stokes, M. J. Higgins, A. P. Kushnick, S. Bhattacharya, and M. O. Robbins, Phys. Rev. Lett. **65**, 1885 (1990).
[5] M. Fourar and S. Bories, Int. J. Multiphase Flow **21**, 621 (1995).
[6] R. J. Glass and M. J. Nicholl, Geophys. Res. Lett. **22**, 1413 (1995).
[7] J. Schmittbuhl, A. Hansen, H. Auradou, and K. J. Måloy, Phys. Rev. E **61**, 3985 (2000).
[8] T. C. Rasmussen, Geophys. Res. Lett. **22**, 1401 (1995).
[9] J. R. Murphy and N. R. Thomson, Water Resour. Res. **29**, 3453 (1993).
[10] *Flow and Contaminant Transport in Fractured Rock*, edited by J. Bear, C. F. Tsang, and G. de Marsily (Academic, San Diego, 1993).
[11] H. Auradou, K. J. Måloy, J. Schmittbuhl, and A. Hansen, Transp. Porous Media **50**, 267 (2003).
[12] M. Latva-Kokko and D. H. Rothman, Phys. Rev. E **71**, 056702 (2005).
[13] G. R. McNamara and G. Zanetti, Phys. Rev. Lett. **61**, 2332 (1988).
[14] F. J. Higuera and J. Jimenez, Europhys. Lett. **9**, 663 (1989).
[15] Y. Qian, D. d'Humières, and P. Lallemand, Europhys. Lett. **17**, 479 (1992).
[16] D. H. Rothman and S. Zaleski, *Lattice Gas Cellular Automata* (Cambridge University Press, Cambridge, 1997).
[17] U. D'Ortona, D. Salin, M. Cieplak, R. B. Rybka, and J. R. Banavar, Phys. Rev. E **51**, 3718 (1995).
[18] A. K. Gunstensen, D. H. Rothman, S. Zaleski, and G. Zanetti, Phys. Rev. A **43**, 4320 (1991); A. K. Gunstensen and D. H. Rothman, Europhys. Lett. **18**, 157 (1992).
[19] I. Ginzbourg and P. M. Adler, J. Phys. II **4**, 191 (1994).
[20] A. Gunstensen, Ph.D. thesis, MIT, Cambridge, 1992.
[21] J. Rowlinson and B. Widom, *Molecular Theory of Capillarity* (Calendon, Oxford, 1982).

[22] U. Frisch, D. d'Humières, B. Hasslacher, P. Lallemand, Y. Pomeau, and J.-P. Rivet, Complex Syst. **1**, 648 (1987).
[23] J. Koplik and J. Banavar, Annu. Rev. Fluid Mech. **27**, 257 (1995).
[24] F. M. White, *Fluid Mechanics* (McGraw-Hill, New York, 1994).
[25] A. Mazouchi and G. M. Homsy, Phys. Fluids **13**, 1594 (2001).
[26] P. Concus and R. Finn, Acta Math. **132**, 177 (1974).
[27] H. Wong, S. Morris, and C. J. Radke, J. Colloid Interface Sci. **148**, 71 (1992).
[28] R. Lenormand, C. Zarcone, and A. Sarr, J. Fluid Mech. **135**, 337 (1983).